NOTE ON THE SPHERE MOTION IN CONFINED GEOMETRY

István MAGOS[1], Corneliu BALAN[2]

The paper communicates an experimental study of sphere motion in confined domains. The sphere is falling free under gravity in square-cross glass vessels filled with a viscous Newtonian liquid. The dynamics are analyzed using the image processing of direct visualizations of the sphere's displacement recorded with a high-speed camera. The corresponding velocity of the sphere and the drag coefficient C_x are calculated for the experiments performed. The following perturbations on the sphere motion are investigated: (i) the wall influence, (ii) the end-effect induced by the bottom wall of the domain, (iii) the presence of free surface/air cavities, and (iv) the sphere's acceleration. The results are original since these phenomena are scarcely analyzed in literature, even though the sphere motion is a classical topic in fluid mechanics.

Keywords: sphere motion, viscous fluid, drag coefficient, Reynolds number

1. Introduction

The sphere motion in viscous fluids is the most studied and investigated subject in fluid mechanics and rheometry. It is probably the main benchmark problem for any scientist working in the fundamental or applied domains where the interaction between a body and a fluid is important. The flow of the viscous fluid generated by the motion of a sphere was first modeled by Stokes at the middle of the XIX century, [1]. Remarkable contributions on the subject were made by Boussinesq [2], and at the beginning of the last century by Allen [3], Einstein in his PhD thesis [4], Oseen (1910) and Goldstein (1929), [5]. The analytical solution of Stokes at low Reynolds number ($Re << 1$), and its extension by Oseen and Goldstein ($Re < 2$), are present in almost all advanced fluid mechanics lecture notes, started with Lamb's book [6] (1st edition published in 1916), see also [7] for a reference in Romanian.

The experimental data related to flows around spheres were obtained by numerous scientists, we mention here the Prandtl's group from Göttingen [8] and the references from

[1]Ph.D. student, REOROM Laboratory, NUST POLITEHNICA Bucharest, Romania, e-mail: istvan.magos@upb.ro
[2]Professor, REOROM Laboratory, NUST POLITEHNICA Bucharest, Romania, e-mail: corneliu.balan@upb.ro

Churchill [9]. The forces acting of rigid spheres falling in viscous liquids at low Reynolds numbers, especially the drag in relation to settling velocity, were intensively investigated in the last decades of the XX century, e.g. [10], [11], [12], the topic being recently reviewed, [13], [14]. Numerous numerical solutions of flows around spheres have been published in relation to vary applications: testing novel numerical techniques [15], heat transfer [16], [17], turbulence [18].

It is important to mention that investigations and solutions of the flows around sphere consider often the fluid domain infinite, the influence of walls on the sphere motion and drag being scarce under investigations. The corrections introduced to the drag Stokes formula by the confined geometry are presented by Happel & Brenner [19], one on the most cited classical book dedicated to hydrodynamics at low Reynolds numbers.

The communication is focused on the visualizations, measurements and computation of the sphere's velocity, falling free in a confined geometry filled with a viscous Newtonian liquid. The main aim of the work is to establish an experimental procedure to determine the influences of the walls and free surface on the drag coefficient of spheres.

2. Experimental

In a quasi-stationary isothermal flow, the one-directional equilibrium of forces acts on a falling sphere under gravity in a Newtonian fluid (viscosity $\eta_0 = \text{constant}$) is given by the relation:

$$F_x = F_G - F_A, \tag{1}$$

where the drag force has the expression,

$$F_x = \frac{C_x}{2}\rho_0 \pi R^2 v_0^2. \tag{2}$$

Here $F_G = \rho_s g V$ is the weight of the sphere, $F_A = \rho_0 g V$ is the bouyancy force, ρ_0 is the fluid density, ρ_s is the sphere density, V is the sphere volume and $d = 2R$ is its diameter, Fig. 1.a. In (2) v_0 is the constant velocity of the sphere and C_x is the drag coefficient.

It is important to remark that relation (1) becomes more complicated in the case of non-stationary sphere motion (i.e. the sphere's velocity is not constant – $\dot{\boldsymbol{v}} \neq 0$),

$$\rho_s V\, \dot{\boldsymbol{v}} = \boldsymbol{F}_\mathrm{G} - \boldsymbol{F}_\mathrm{A} - \boldsymbol{F}_x - \boldsymbol{F}_{ma} - \boldsymbol{F}_B, \tag{3}$$

where three supplementary forces are present, [10-13] : (i) sphere inertia (left term), (ii) $\boldsymbol{F}_{ma} = (\rho_0/2) V\, \dot{\boldsymbol{v}}$, added mass force (generated by unsteady pressure distribution around sphere), (iii) $\boldsymbol{F}_B = (3/2) d^2 \sqrt{\pi \rho_0 \eta_0} \int_0^t \frac{\dot{v}(\xi)}{\sqrt{t-\xi}} d\xi$ the Basset force

induced by the transitory friction in boundary layer (generated by unsteady shear stress over sphere), [14, 20, 21].

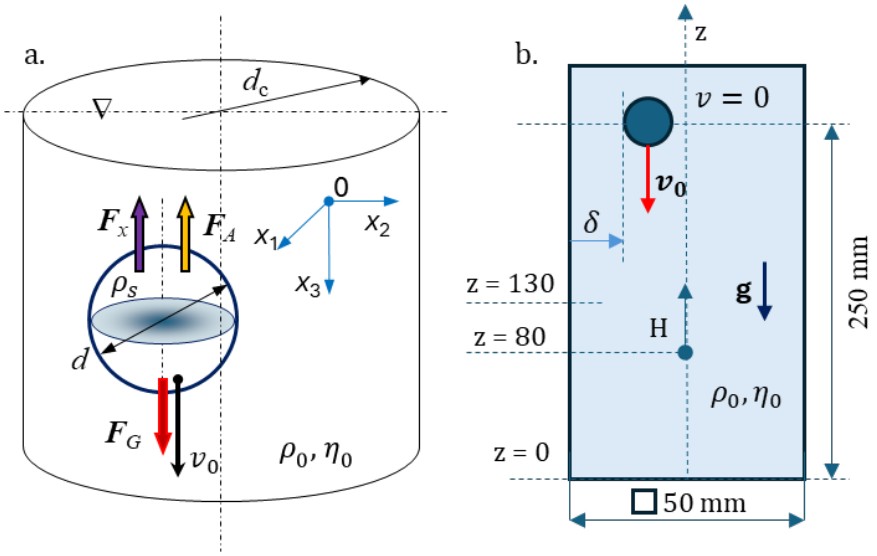

Fig. 1. a) Forces acting on a sphere in motion with constant velocity v_0 in a vertical tube with diameter d_c; b) laboratory test configuration; the sphere is located on one axis of symmetry of the square cross-section vessel (the sphere is falling free along the vertical coordinate $z = -x_3$).

The measure of the drag force is the drag coefficient C_x. In a steady motion, C_x depends on the Reynolds number $Re = \rho_0 d v_0/\eta_0$ and on the configuration of the flow domain [19],

$$C_x(Re, d/d_c, \delta/d_c, \varepsilon/d\,), \tag{4}$$

Fig. 1, respectively. In (4) ε is the distance of the sphere from the bottom-wall of the domain.

In the case of an infinite domain, $d_c \to \infty$, far away for any walls, $\varepsilon \to \infty$, the drag coefficient for steady motion depends exclusively on the Reynolds number. The solution was obtained by Stokes [1, 6, 7] at $Re \ll 1$, $C_{x0} = 24/Re$, respectively; only in this hypothesis the drag force has an exact analytical solution, $F_x = 3\pi\eta_0 d v_0$, which was used also by Eistein to calculate the diffusion coefficient of the solute in a solvent, [4]. We mention that Stokes solution was obtained by integration of the stresses distribution (pressure and viscous shear) on the sphere surface, where the fluid adheres.

Approximative solutions of the dependence $C_x(Re)$ at small ($Re < 3$) and medium ($Re < 1000$) Reynolds numbers are shown in literature [5, 7, 19], e.g.

$$C_x^* = C_{x0}\left(1 + Re^{2/3}/6\right), \tag{5}$$

[22]. However, in the laminar flow regime the decreasing of drag coefficient with Reynolds number follows with a fair approximation the power law function,

$$C_x \sim Re^{-n}. \quad (6)$$

Experimental diagrams for the whole range of Reynolds numbers, from laminar (including Stokes flows) to developed turbulence, can be found in any applied fluid mechanics lectures, [9]. Excepting few publications, [19], and published numerical solutions, [23, 24], there are no available data for the dependence of drag coefficient on Reynolds number in confined geometries.

It is assumed that forces $\boldsymbol{F}_{ma}$ and $\boldsymbol{F}_B$ have a minor influence in our case, therefore the expression form (3) of the drag coefficient is given by,

$$C_{xi} = \frac{4d}{3\rho_0 v^2}(\Delta\rho g - \rho_s a), \quad (7)$$

where the sign of acceleration $a = \dot{v}$ is negative in the case of deceleration.

The experiments performed in the REOROM laboratory used a steel sphere with diameter
$d = 10\ mm$ and mass $m = 4.08\ g$ (corresponding density $\rho_s \cong 7800$ kg/m^3). The sphere is dropped in glass vessels with square cross sections $b \times b$ (b = 30 mm and b = 50 mm, respectively; 275 mm height, the thickness of the assembled glass walls being 3 mm), filled with a Newtonian silicone oil: density $\rho_0 = 960$ kg/m^3 and viscosity $\eta_0 = 0.98$ Pas. The visualizations of the sphere motion in the fluid sample were obtained with a high-speed camera: Phantom VEO-E 340L at 2800 fps (resolution 1024x1024 pixels, pixel size 10 microns). All experiments were performed at a temperature of 23^o C (room temperature in the laboratory).

Photos at prescribed times are extracted from the movies, Fig. 2, the sphere's advance H(t) inside the liquid is measured, and the corresponding falling velocity is calculated, $v(t) = \dot{\mathrm{H}}(t)$, Fig. 3. Finally, the dependences $C_x(Re)$ are represented for the analyzed cases.

2.1 Wall influence

In the flow configuration from Fig. 1.b the immersed sphere is dropped from z = 250 mm, with initial velocity $v(0) = 0$, at different distances δ from the wall, Tab. 1. The position of the sphere on z-axis is recorded in the interval $z \in [80, 130]$ mm, H $\in [0, 50]$ mm respectively.

During tests the distance of the sphere to the vessel's lateral walls is maintained constant, the displacement of sphere within the fluid being measured by processing the images extracted from the recorded movies at certain moments of time. In Fig. 2 are represented four images for a sphere falling in the very vicinity of the wall ($\delta \cong 0$).

In Fig. 3 the measured heights H(t) and the corresponding falling velocities of the spheres are represented, where the origin of time, t = 0, corresponds to the height H = 0 (z = 80 mm), where steady velocity v_0 is reached, Fig. 1b. The

dependences H(t) are almost linear, the velocities being slightly increasing with z-coordinate decreasing. With fair approximation one can consider the flow regime in the recorded interval as quasi-stationary.

The values for the Reynolds number and the drag coefficient are shown in Tab. 1. It is observed from Fig. 3 that for $\delta > 10$ mm the velocity of the sphere is nearly constant (the middle of the vessel corresponds to $\delta = 25$ mm).

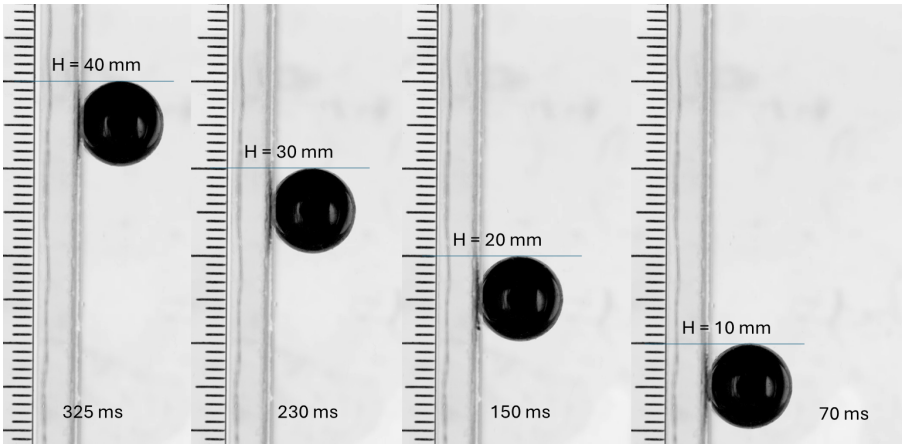

Fig. 2. Series of photos of the falling sphere in the very vicinity of the walls; corresponding between height H and time t (the sphere sliding at the corner of the vessel, $\delta \cong 0$, case a_{00} in Fig. 3). The dark lines are shadows of the transparent glass walls, the ruler being attached to the wall outside the vessel.

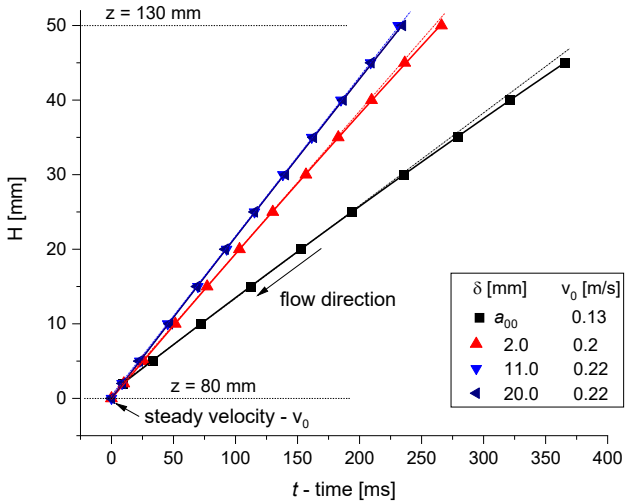

Fig. 3. Dependences H(t) and the steady values v_0 of velocity as function of the sphere's distance from the wall (case a_{00} corresponds to the corner of the vessel). Velocity of the sphere is slightly increasing to v_0 from H = 50 mm to H = 0 mm (the linear dependence H(t) is represented with dash line), so the influence of acceleration is not relevant in this case.

Table 1.

The values of the quasi-steady velocity, Reynolds number and the drag coefficients. The values of C_x are calculated assuming constant velocity, i.e. $a = 0$ in (7).$\boldsymbol{\delta}$ wall t

$\boldsymbol{\delta}$ wall distance	a_{00} – corner	2 [mm]	11 – 20 [mm]
$\boldsymbol{v_0}$ [m/s]	0.13	0.2	0.22
$\boldsymbol{Re}$ [-]	1.27	1.95	2.16
$\boldsymbol{C_{x0} = {}^{24}/_{Re}}$ [-]	19	12.3	11.0
$\boldsymbol{C_x^* = C_{x0}(1 + Re^{2/3}/6)}$	22.7	15.48	14.05
$\boldsymbol{C_x}$ **[-]**	55	23.2	19.2
$\boldsymbol{C_x/C_x^*}$	2.4	1.5	1.36
$\boldsymbol{C_x/C_{x0}}$	2.9	1.9	1.75

The drag coefficient C_x is decreasing with increasing *Re*-number and the distance from the wall of the vessel. The ratio C_x/C_{x0} is 2.9 at the wall and 1.75 in the center of the vessel. The correction due to Reynolds number, (5), increases C_{x0} with factor 1.27 in the center, therefore the confined square geometry increases the drag coefficient calculated for an infinite domain with factor 1.36 relative to C_x^* and 1.76 relative to C_{x0}, respectively. There are no available data in literature for a square flow section, but for a circular section, Fig. 1.a, $C_x \cong 1.68 \cdot C_{x0}$ for $d/d_c = 0.2$ (in our experiments $d/b \cong 0.2$) assuming a perfect concentricity of the sphere with the cylindrical wall and $Re < 1$, [19]. Appling the two corrections to C_x in the center of the domain, one can remark that measurements give a fair estimation of the confinement influence on the sphere motion, i.e. $C_x = 19.2$ (measured value) against $C_x \cong 18.48$ (approximative value calculated from literature, [19]).

2.2 End effect influence

The end-effect is observed in the vicinity of the bottom wall of the vessel, where the sphere's velocity is decreasing from the steady velocity v_0 to the settle (impact with the bottom) velocity v_s. The sphere is launched in a vessel with a square-cross section, b = 30 mm, filled with fluid up to z = 175 mm. The impact velocity of the sphere on the free surface is $v_i \cong 1.4$ m/s and its motion are recorded

starting at $t = 0$ from H = 60 mm (where steady velocity is reached), H = 0 defining in this experiment the bottom of the vessel, Fig. 4. In Fig. 5 the measured heights H(t) and the corresponding calculated velocities are represented.

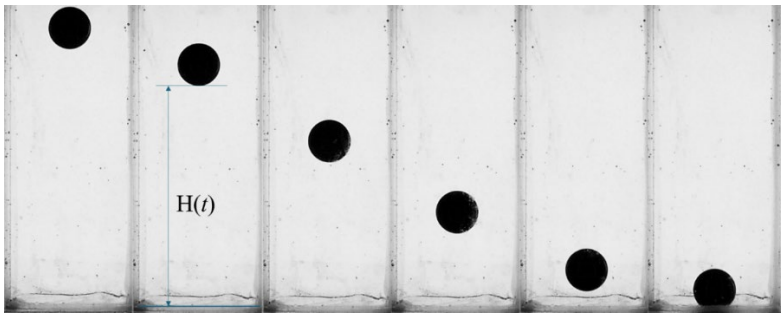

Fig. 4. Selection of images in the interval of 0.42 s.

Two flow regimes are observed in Fig. 5: (i) a steady state flow with constant velocity $v_0 \cong 0.147$ m/s, (ii) a decelerating flow in the vicinity of the bottom, from v_0 to $v_s \cong 15$ mm/s in 0.065 s. The transition between the regimes is marked in Fig. 5, region A-B, respectively. We notice that deceleration in the vicinity of the bottom is $a \cong -4.5$ m/s^2, which has an important influence on the value of C_x in the vicinity of the bottom wall where the motion is unsteady, (7).

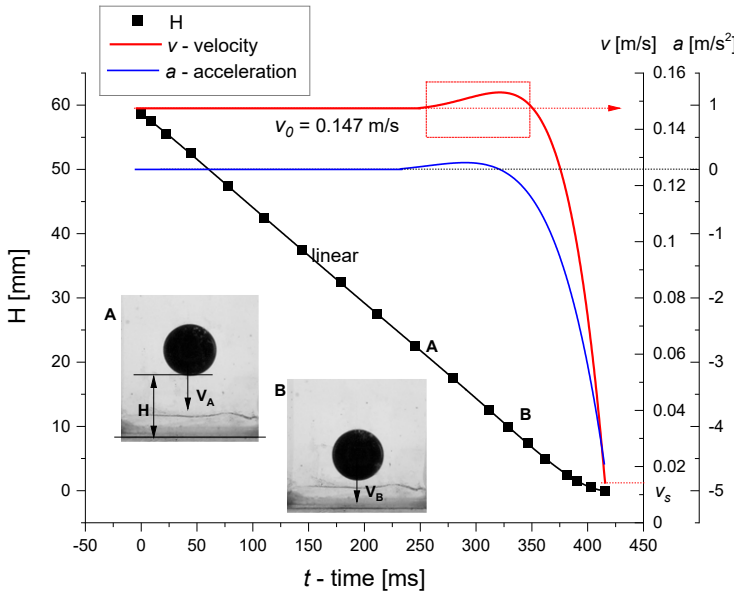

Fig. 5. Time variation of the distance from the bottom wall and the calculated falling velocity of the sphere. A slight increase of velocity is observed before the sharp decreasing in the very vicinity of the bottom wall.

2.2 End effect and free surface influences

The sphere is launched in a vessel with a square-cross section, b = 50 mm, with impact velocity $v_i \cong 2.5$ m/s on the free surface corresponding to H = 60 mm from the bottom, Fig. 6. In this experiment the origin of time, t =0, corresponds to the impact of sphere on the free surface, which corresponds to the distance H = 60 mm from the bottom (H = 0). The dynamics of the air cavity formed down-stream the sphere and the rupture/pinch-off of the air filament are studied by the authors in [25].

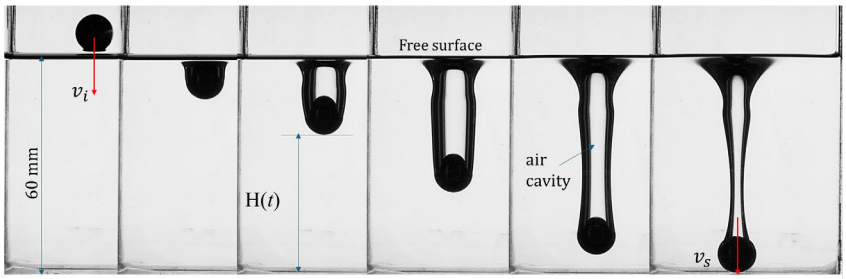

Fig. 6. The falling of the sphere and the formation of the air-cavity in 47 ms.

The experimental dependences H(t) and $v(t)$ from Fig. 7 are very good fitted by an exponential decreasing function, with slightly deviations in vicinity of the free surface and in the region where the end-effect is present. One can consider that velocity is decreasing continuously from $v_i \cong 2.2$ m/s to $v_s \cong 0.55$ m/s (settle velocity), therefore deceleration influences C_x for the whole analyzed time interval. In Fig. 8 are represented the Stokes formula $C_{x0} = 24/Re$, $C_x^*(Re)$ from (5), both valid for infinite flow domain, $C_x(Re)$ calculated without contribution of inertia and $C_{xi}(Re)$ with inertia, (7). The values of n-exponent from (5) are also shown.

The analysis of the results from Fig. 8 evidence cumulated effects on the dynamics of sphere: (i) confinement of the flow domain, (ii) unsteady motion, (iii) end effect, (iv) presence of free surface and air cavity. These mentioned influences are present in almost all applications where motions of immersed spherical bodies are under study, so the formulas for drag coefficients published in literature have to be used with caution (especially if the spherical surface is not smooth, it is not hydrophilic or there are deviations from perfect sphericity).

The end effects in the absence and in the presence of free surface are compared in Fig. 9, where the dependences $C_x(Re)$ and H(Re), calculated from experimental data (Fig. 5 and Fig. 7, respectively), are shown.

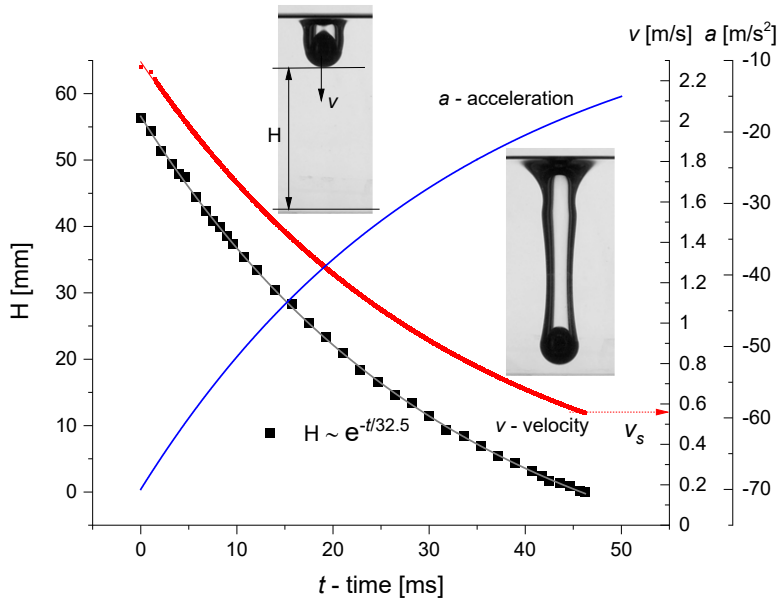

Fig. 7. Time variation of the sphere distance and velocity from the impact on the free surface to the bottom wall.

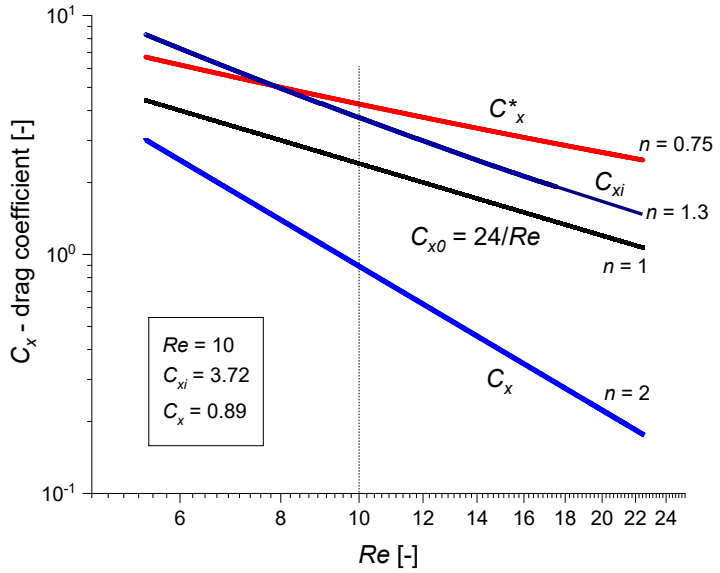

Fig. 8. Dependence of drag coefficients on the *Re*-number (experimental data from Fig. 7).

There are qualitative and quantitative differences between the cases from Fig. 9 (in cross section of the vessel and impact velocities, absence or presence of air cavities, steady or unsteady sphere motion), but we also observe two important similarities, even though data in the interval $1.5 < Re < 5$ are missing: (i) the decreasing of the calculated drag coefficient C_x with *Re*-number has the same *n*-

index (i.e. same slope), (ii) the end-effect is relevant in a boundary zone situated in both cases ~~at~~ for H < 5 mm. We must mention that inertia contribution to the drag coefficient is more relevant if the air cavity remains attached to the sphere, Fig. 8, e.g. $C_{xi} \cong 4.18C_x$ at $Re = 10$.

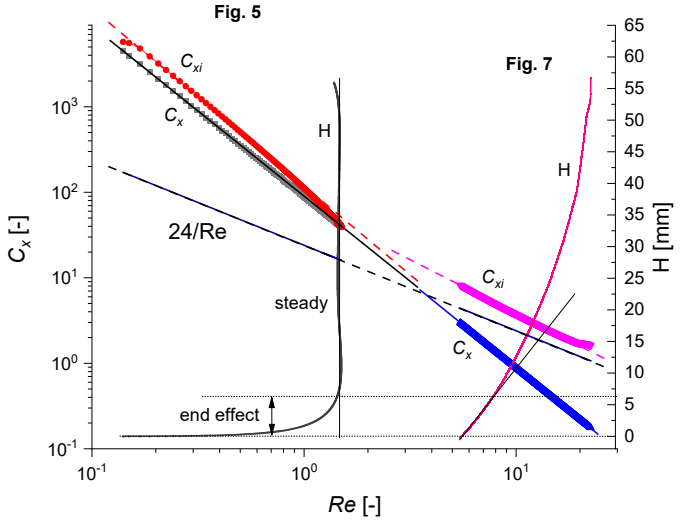

Fig. 9. Experimental $C_x(Re), C_{xi}(Re)$ and $\mathrm{H}(Re)$ from Fig. 5 and Fig. 7 (free surface influence).

One concludes that motion of the sphere in the vessel is influenced by the lateral confinement (wall effect), by the bottom wall (end effect) and inertia. These effects at small and medium *Re*-numbers increase the drag coefficient and the *n*-index in comparison to the formulas for an infinite domain.

3. Final remarks and conclusions

The paper is an experimental study focused on measuring different influences on the sphere motion in a confined domain filled with a Newtonian viscous liquid. The procedure is based on the
image processing of direct visualizations of the sphere's displacement recorded with a high-speed camera. The corresponding velocity of the sphere and the drag coefficient C_x are calculated directly from experiments, without solving the Navier-Stokes equations in the fluid domain.
The following influences on sphere motion are investigated: (i) vicinity of the wall, (ii) end-effect induced by the bottom wall of the domain, (iii) the presence of free surface and air cavity, and (iv) sphere's acceleration.

In the range of small and medium Reynolds numbers, $0.01 < Re < 20$, the results evidence that any influence of the confinement (wall effect and end effect) on the sphere motion determines the increasing of the drag coefficient. This finding

is expected and known, [13, 14, 19, 23, 24], but results based on experiments performed in confined geometries with square cross section and in the presence of free surface were not reported in literature. This is the original contribution of the author and brings complementary valuable results to this extensively studied phenomenon in applied fluid mechanics: the motion of spherical bodies in viscous liquids. One main conclusion of the work is to use in applications with caution the formulas for drag coefficients, especially for analyzed motions where influences of the flow confinement and air cavities are evident. This is always the case when the study is focused on determining the influence of fluid's properties on the displacement of immersed bodies.

The confined geometry defines the domain and imposes the boundary conditions for the flow generated by the falling sphere in the fluid. For a given flow domain (i.e. boundary conditions) filled with a non-Newtonian fluid, in particular viscoelastic, the drag coefficient of the sphere depends not only on the Reynolds number (and Strouhal number for unsteady/oscillatory flows, [9]), but also on parameters associated with the complex rheology of the fluid (as relaxation time, [26]). In principle, the drag coefficient can be calculated by integrating on the sphere the pressure and wall shear stress distributions obtained from the numerical solution of the equations of motion for a particular fluid model (constitutive relation), [24, 26]. Motion of spheres in viscoelastic fluids is an important domain of study, with numerous applications in modelling complex flows, interfacial dynamics and transport of particles in microgeometries, [23, 27, 28, 29, 30]. Experimental investigations of the steel spheres' impact on viscoelastic fluids in the presence of magnetic field are in progress at the REOROM laboratory from Politehnica University, [31].

Acknowledgements

The authors acknowledge the financial support of CHISTERA-19-XAI-009 MUCCA Project, by the founding of EC and the Romania Executive Agency for Higher Education, Research, Development, and Innovation Funding—UEFISCDI, Grant COFUND-CHIST-ERA No. 206/2019.

REFERENCES

[1] *G. C. Stokes*. On the effect of the internal friction of fluids on the motion of pendulums. 1851. Trans. Camb. Phil. Soc. Part II, 9:8-106.

[2] *V. J. Boussinesq*. Sur la résistance qu'oppose un liquide indéfini au repos au mouvement varié d'une sphère solide. 1885. C. R. Acad. Sci. Paris 100, 935-937.

[3] *H. S. Allen.* The motion of a sphere in a viscous fluid. 1900. L.E.D. Phil. Magazine and J. of Science 50(306), 519-534.

[4] *A. Einstein*. On the motion of small particles suspended in liquids at rest required by the molecular-kinetic theory of heat. 1905. Annalen der Physik 17, 549-556.

[5] *W. E. Langlois*. Slow viscous flows. 1964. Macmillan Comp. New York. pp. 131-155. Corrections Re

[6] *H. Lamb*. Hydrodynamics. 1945. 6th edition, Dover, New York. pp. 602-604

[7] *T. Oroveanu*. Mecanica fluidelor vîscoase. 1967. Ed. Academiei, București. pp. 187-201

[8] *E. Bodenschatz and M. Eckert*. Prandtl and the Göttingen school. 2011. in: Davidson PA, Kaneda Y, Moffatt K, Sreenivasan KR, eds. A Voyage Through Turbulence. Cambridge Univ. Press, pp.40-100.
[9] *S. W. Churchill*. Viscous flows – the practical use of theory. 1988. Butterworths, Boston. pp. 388 – 405.
[10] *F. Odar and W. S. Hamilton.* Forces on a sphere accelerating in a viscous fluid. 1964. J. Fluid Mech. 18, 302-314.
[11] *R. G. Cox*. The steady motion of a particle of arbitrary shape at small Reynolds numbers. 1965. J. Fluid Mech. 23, 625-643
[12] *P. M. Lovalenti and J. F. Brady.* The hydrodynamic force on a rigid particle undergoing arbitrary time-dependent motion at small Reynolds number. 1993. J. Fluid Mech. 256, 561-605.
[13] *P. P. Brown and D. F. Lawler*. Sphere drag and settling velocity revisited. 2003. J. Environmental Eng. 129(3), 222-231.
[14] *J. Guo*. Motion of spheres falling through fluids. 2011. J. Hydraulic Research . 49(1), 32–41.
[15] *I. Rodriguez, R. Borell, O. Lehmkuhl, C. D. Perez Segarra and A. Oliva.* Direct numerical simulation of the flow over a sphere at *Re* = 3700, 2011, J. Fluid Mech. 679, 263 – 287.
[16] *R. Kurose, M. Anami, A. Fujita and S. Komori*. Numerical simulation of flow past a heated/cooled sphere. 2012. J. Fluid Mech. 692, 332-346.
[17] *Z. Duan, B. He and Y. Duan.* Sphere drag and heat transfer. 2015. Scie. Rep. 5, 12304.
[18] *W. Shang, H. Zhao, D. Li, K.H. Luo and J. Fan*, Direct numerical simulation of the flow around a sphere immersed in a flat-plate turbulent boundary layer. 2021. Physics Fluids 33(11), 115106.
[19] *J. Happel and H. Brenner H*. Low Reynolds number hydrodynamics with special applications to particulate media.1965. Prentice-Hall, Englewood Cliffs. pp. 286-357.
[20] *E. Limacher, Ch. Morton and D. Wood.* Generalized derivation of the added-mass and circulatory forces for viscous flows. 2018. Phys. Rev. Fluids 3, 014701
[21] *E. J. Limacher*. Added-mass force on elliptic airfoils. (2021). J. Fluid Mech. 926, R2.1-11.
[22] *A. Putnam*. Integrable form of droplet drag coefficient. 1961. ARS Journal 31, 1467-1468.
[23] *R.G.M. van der Sman*. Drag force on spheres confined on the center line of rectangular microchannels, 2010, J. Colloid Int. Scie. 351, 43-49.
[24] *S.A. Faroughi, C. Fernandes, J. Miguel Nóbrega and G.H. McKinley*. A closure model for the drag coefficient of a sphere translating in a viscoelastic fluid, 2020, J. Non-Newtonian Fluid Mech. 277, 104218.
[25] *I. Magos and C. Balan.* Experimental investigations of air-cavity formation in viscous and viscoelastic liquids.2024. Phys. Fluids 36, 093103.
[26] *G. D'Avino, G. Cicale, M.A. Hulsen, F. Greco and P.L. Maffettone*. Effects of confinement on the motion of a single sphere in a sheared viscoelastic liquid. 2009. J. Non-Newtonian Fluid Mech. 157, 101-107.
[27] *B. Akers and A. Belmonte.* Impact dynamics of a solid sphere falling into a viscoelastic micellar fluid. 2006. J. Non-Newtonian Fluid Mech. 135, 97–108.
[28] *P. Akbarzadeh, M. Norouzi, R. Ghasemi and S. Z. Daghighi*. Experimental study on the entry of solid spheres into Newtonian and non-Newtonian fluids. 2022. Phys. Fluids 34, 033111.
[29] *C. Liu, C. Xue, J. Sun and G. Hu*. A generalized formula for inertial lift on a sphere in microchannels. 2016. Lab Chip 16, 884-892.
[30] *C. Ye and D. Li*. Electrophoretic motion of a sphere in a microchannel under the gravitational field, 2002, J. Colloid Int. Scie. 251, 331-338.
[31] *C. Mateescu, I. Magos and C. Balan*. Drag coefficient of spheres at the interface between air and viscoelastic fluids. 2025. in preparation for publication (oral communication at AERC 2025, 14 -17 April, Lyon).